Optical focusing beyond the diffraction limit via vortex-assisted transient microlenses

*Eitan Edrei And Giuliano Scarcelli**

Fischell Department of Bioengineering, University of Maryland, College Park, Maryland 20742, USA
**Corresponding author: scarc@umd.edu*

Focusing light beyond the diffraction limit is among the greatest challenges in optical sciences, which would revolutionize many optical technologies from imaging and optical trapping to light delivery and photomedicine. To achieve sub-diffraction focusing, metamaterials, materials with engineered scattering properties, or attached microspheres have been proposed. Here we introduce a new paradigm to achieve a physical focus beyond the diffraction limit without additional optical elements or exogenous labels, but only using light-matter interactions. We spatially control light absorption within the focal region of a lens to generate a transient heat source and sculpt a semi-parabolic refractive index pattern within the sample itself. This effectively generates a converging microlens with a focusing spot below the diffraction limit of the optical system that can be used for super-resolution imaging by scanning the spot across the sample. Our method is broadly compatible with imaging and focusing systems used in many applications.

In the past twenty years, in imaging applications, localization techniques[1, 2] and stimulated emission[3] have been able to overcome the diffraction limit by exploiting the chemical properties of fluorophores. However, in these methods, light is not physically focused beyond the diffraction limit; this reduces the application space by requiring labelling, complex sample preparation and/or imposing strong intensity and speed limitations. Instead, focusing light beyond the diffraction limit remains an open challenge which would revolutionize a wide range of applications from imaging and optical trapping to light delivery and photochemistry.[4, 5] By pre-engineering or pre-characterizing the scattering properties of materials, several works have demonstrated progress towards sub-diffraction imaging and focusing, yet with intrinsic limitations of alignment and pre-characterizations.[6, 7] The discovery of metamaterials[8, 9] enabled the design of super-lenses which are capable of sub-diffraction imaging by enhancing the evanescent field typically lost otherwise.[10] Recently, the introduction of microspheres in the vicinity of an object has been shown to provide sub-wavelength resolution by curving the incident and reflected rays[11, 12]. Yet, in these modalities, an external optical element needs to be placed very close to the imaged object, which also dramatically reduces the broad applicability of the techniques.[13] Here we introduce a scheme capable of focusing light to a sub-diffraction spot by exploiting the refractive index variations induced by light-matter interactions. Such focal confinement can be used to efficiently deliver light to photoactive nanostructures, to perform super-resolution imaging without labels, as well as to perform spectroscopic measurements at higher resolutions than those offered by the optical system.

PRINCIPLE

The principle of the proposed technique is schematically shown in Figure 1a. To achieve tight focusing of a probe beam (green), negligibly absorbed by the sample, we use an auxiliary beam (red) of different wavelength, which is strongly absorbed by the sample. In water-based solutions, the temperature

dependence of the refractive index is negative (i.e. $\frac{dn}{dT} < 0$). Therefore, the auxiliary beam is shaped by a vortex phase plate to generate transient absorption in the shape of a donut, i.e. a ring with a diffraction limited void at the center. This heat profile induces a refractive index gradient at the waist of the focusing lens with highest index at the center of the ring and monotonically decreasing towards the periphery. This process effectively sculpts a transient converging microlens with diameter equal to the optical diffraction limit. Thus, when the probe beam passes through the sculpted microlens (either collimated or focused), it will converge to a tighter focal point than what is allowed by the optical system, as shown experimentally in Figure 1b. The smaller focal point can be used as a scanning probe for imaging at superior resolution (Figure 1c) without any labeling process or material insertion, providing high flexibility of the optical configuration.

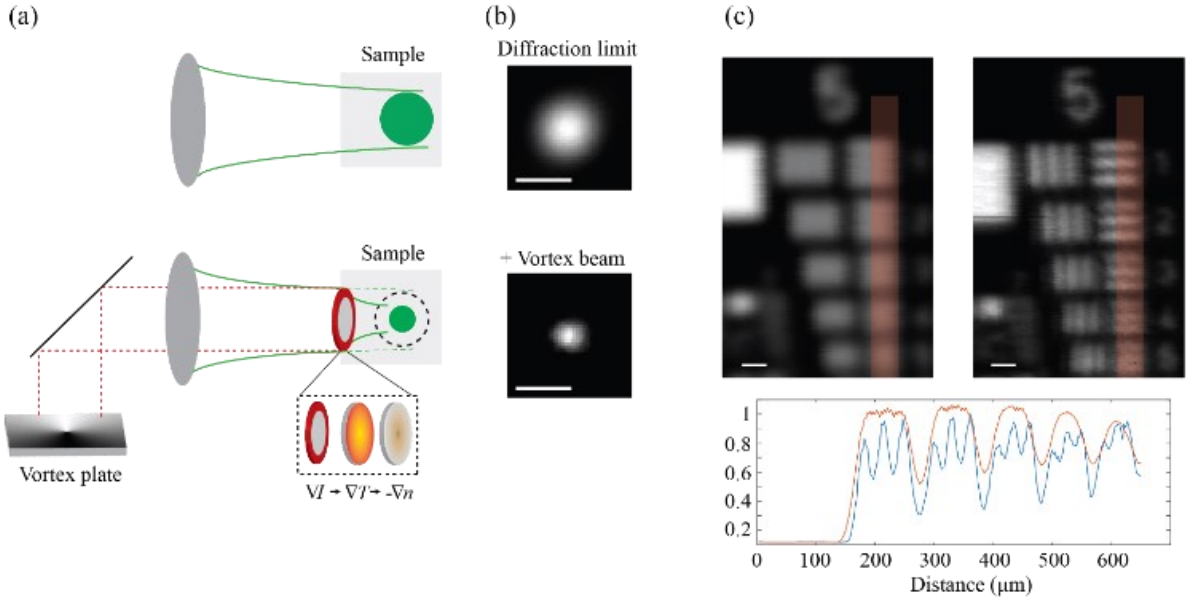

Fig. 1: (a) Schematics of the vortex-assisted focusing. (b) Experimental comparison between the diffraction-limited spot and the one obtained via vortex assisted focusing (Scale Bar, =30 μm). (c) Scanning microscopy image of USAF resolution chart with (left) and without (right) the vortex plate (scale bar = 30 μm). Image resolution is enhanced as can be quantitatively seen from the line plot of the marked region (bottom).

The demonstrated sub-diffraction focusing is the result of a thermal nonlinear effect that can be described mathematically by considering the temperature effect on the refractive index given by:[14]

$$n(r,t) = n_0 + \left(\frac{dn}{dT}\right) T(r,t) \qquad (1)$$

where $T(r,t)$ is the temperature distribution in the material. In our proof-of-principle experiment, we achieved focusing in the millisecond time scale (limited by the available laser intensity) and thus the temperature distribution in the material needs to be evaluated from the solution of the heat diffusion equation with a given set of initial and boundary conditions dictated by the absorbed light pattern and the geometrical configuration. However, high intense pulsed lasers would enable operating in thermal confinement regime where heat diffusion can be neglected, and the temperature distribution will closely follow the light beam profile.

Once the refractive index profile is obtained, the focusing parameters can be calculated from the geometrical ray equation.[15] For a time-varying parabolic profile of refractive index, the focal length can be

shown to follow a power-law scale $F(t)\sim t^{-1}$ and approach the value of (see Supplementary for a full derivation):[16]

$$F(\infty)=\frac{k\pi n_0\omega_0^2}{0.24bPl\cdot\left(\frac{dn}{dT}\right)} \qquad (2)$$

where ω_0 is the beam waist of the physical lens (i.e. the diffraction limited radius in our experiment), b is the absorption coefficient, l is the length of the absorbing cell, k is the thermal conductivity and P is the laser power. If we assume the cell is thick enough to absorb all the light, we can eliminate the product of the absorption coefficient and the cell length since: $b\sim l^{-1}$. Thus, the modulation of the refractive index can be understood as a transient microlens with radius ω_0 and focal length $F(\infty)$ sculpted within the focal region of the physical lens. The resulting spot size $\omega(\infty)$ of such system is dictated by the Abbe diffraction limit of the transient microlens, smaller than the diffraction limit of the physical optical system:

$$\omega(\infty)\approx\frac{\lambda F(\infty)}{2\omega_0} \qquad (3)$$

The final spot size $\omega(\infty)$ depends on the specific material and system parameters. By substituting our experimental parameters (power 0.1W) and material properties, we calculate the expected improvement of the focal size to be $\omega(\infty)\approx 0.4\omega_0$, consistent with our experimental results in Figure 1b.

EXPERIMENTAL SETUP

The experimental setup is presented in Figure 2a. We expanded a monochromatic laser beam of wavelength 1064 nm (La1, Ekspla LightWire FP 200, presented in red) by a set of lenses (L1, f = 50 mm; L2, f = 150 mm). Along the beam path we placed a beam shutter (BS) controlled by a function generator (FG) to determine the duration of the exposure. We transmitted the beam through a phase plate (PP, RPC Photonics, VPP-m1064) and focused it onto the sample (S) using a spherical lens (L4, f = 200 mm) to produce a ring-shaped light pattern. Next, we applied a probe beam of 780 nm (La2, Newport SWL-7513, presented in green) to the sample. For convenience we projected the probe beam through the same limiting aperture as a plane wave, however, it is also possible to focus it to the exact location of the ring-shaped auxiliary beam. The probe beam was introduced using a dichroic mirror (DM) and the lenses L3 (f = 100 mm), L4 as a telescope. The sample was designed to strongly absorb 1064nm but negligibly absorb 780nm. It was produced by mixing 1% of NIR absorbing dye (QCR Solution Corp, NIR1054B, see supplementary for full details and spectrum) in water and placing it in a thin glass chamber. The heat profile generated by the absorption of La1 resulted in a tight focus of La2 right after the absorbing material in a plane indicated by a dashed line. We imaged the transient focusing plane using a 4-f imaging system (not shown) and a camera (C, Andor Zyla 4.2) triggered by the function generator FG. A bandpass filter (BF) was used to block any residual light from La1 not absorbed by the sample. For imaging applications such as presented in Figure 1(c), the object of interest was placed right behind the dye solution at the plane indicated by the dashed line where the focal point is formed and scanned.

RESULTS AND DISCUSSION

Figure 2b shows the experimental focus spot size at three different distances from the vortex location after the sample absorbed a total energy of 1 mJ. The confinement of the focal point is formed as the beam propagates away from the heated region. Accordingly, the signal to background (SBR) value increases as the tighter focal point is formed (figure 2c). Figure 2d shows the focal spot size as a function of increasing energy absorption of the auxiliary beam (and thus heating); the spot size is normalized to the diffraction limit of the optical system (dashed line). The experimental data initially follow the expected power law of $\sim t^{-1}$ as shown by the fit (red line) but slightly deviate from the expected value at $\omega(\infty)$. This deviation

arises from assumptions made to enable the analytical solution of the heat equation and obtain the closed-form expression in Eq. (2), such as an infinite medium model and a parabolic heat profile.

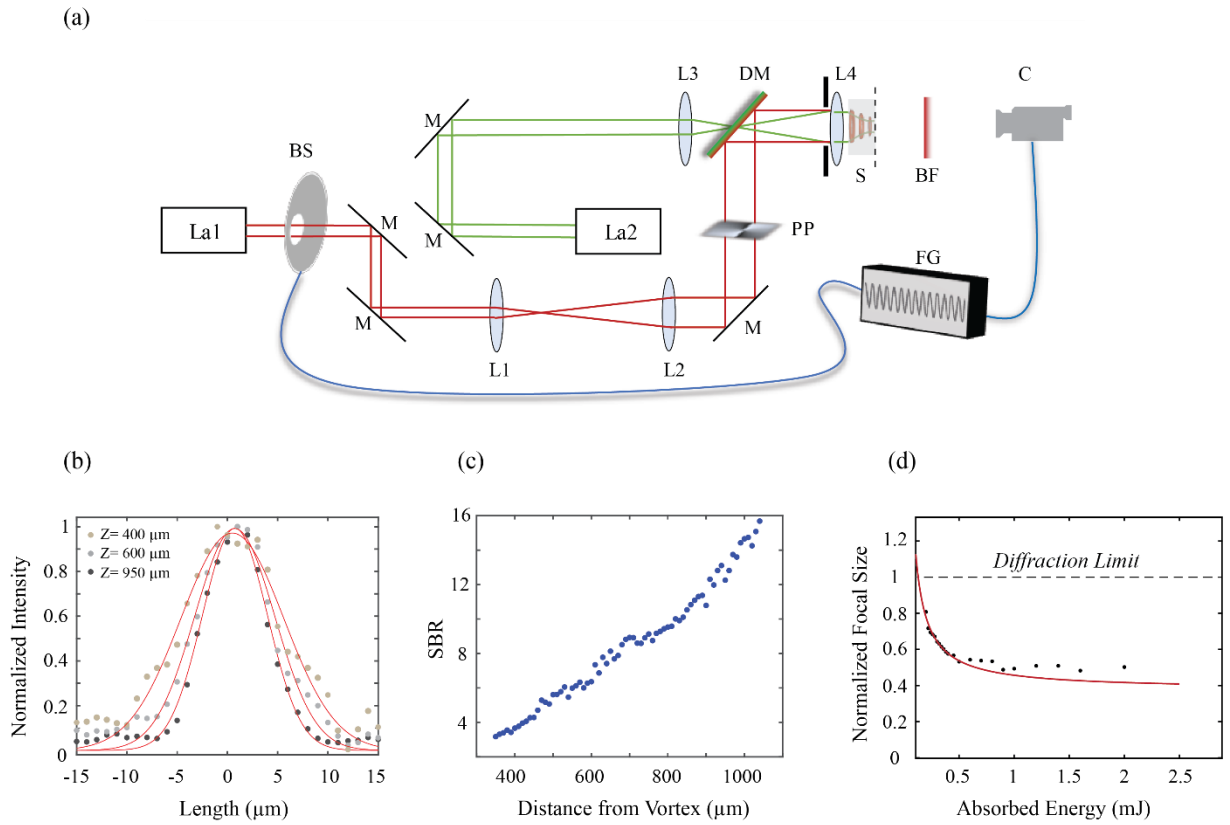

Fig. 2: (a) Experimental setup: Laser (La), Lens (L), Beam Shutter (BS), Function generator (FG), Phase Plate (PP), Dichroic mirror (DM), Sample (S), Filter (BF), Camera (C). (b) Experimental focal spot size at different axial distances from the vortex heat profile (absorbed energy = 1 mJ). (c) SBR values at different axial distances from the vortex heat profile. (d) Focal spot size normalized to the system diffraction limit at increasing energy absorption values (black dots) and a theoretical fit (red line).

Thus, we have performed a proof-of-principle experiment to demonstrate focusing of light beyond the limits of a given optical system without external optical elements or labels using modulation of refractive index within the target material itself. Other strategies to modulate the refractive index of materials to steer optical beam propagation have been previously demonstrated either using high-energy lasers to induce a non-linear effect,[17] or employing acoustic waves to induce a pressure gradient.[18, 19] These approaches would not work for our intended application because of too much energy required or of intrinsic limited spatial resolution, respectively. Thermal lensing effects have been known, but so far they have been primarily used to quantify absorption properties;[20-22] some theoretical studies have discussed the feasibility of generating sub-diffraction signatures for optical writing.[23] Recently, it has been proposed that detected thermal radiation generated by an absorbed focal point can provide sub-diffraction information due to the non-linear nature of blackbody radiation.[24] Here is the first experimental demonstration of focusing and imaging beyond the diffraction limit of a given optical system obtained by detecting the optical radiation modulated by the thermally-induced index gradient.

It is important to discuss the potential of this physical phenomenon to go beyond the focusing limits of currently available high-index immersion objectives. To do so, the heat profile radius needs to be scaled

down to $\omega_0 < 1\ \mu m$, which poses two difficulties: 1. Light absorption needs to occur within the Rayleigh range of the focused vortex ($< 2\ \mu m$), hence, a material/wavelength combination resulting in high absorption is needed. 2. When such a small spatial scale is considered, the stability of the heat profile can become difficult to maintain because of heat diffusion. However, pulsed laser sources of high intensity, and potentially samples with low heat conductivity, can counter these issues by operating in the regime of thermal confinement with much reduced diffusion. It is also possible to use the shorter wavelength as the heat generator and longer wavelength as the probe beam which may allow more efficient heat generation using for instance plasmonic nanoparticles. Yet, one needs to consider the greater susceptibility of shorter wavelengths to scattering as well as the efficiency and availability of materials which can operate using higher wavelengths as probes for photochemical effects or fluorescence microscopy.

A second practical consideration to make, especially for biological applications, is the potential for thermal damage given that the lens sculpting is based on absorption. A common metric to assess tissue damage is the cumulative equivalent minutes at 43^0 (CEM_{43})[25] which for temperature higher than 43 degrees is given by:

$$CEM_{43} = \Delta t \cdot 0.5^{43-T} \qquad (4)$$

where Δt is the exposure time and T is the temperature reached by the sample. Damage thresholds vary between tissue types and species, however, CEM_{43} values between 0-20 minutes typically indicate minor and/or reversible effects. Setting $CEM_{43} = 1$ and considering a short exposure time which can be provided by a ultrafast pulsed laser (e.g. $\Delta t = 100\ fsec$), a temperature of up to 86^0 C (359^0 K) is still under the threshold damage. To estimate the heat profile and the corresponding refractive index map in our experimental setup we performed a heat diffusion simulation of the process. The heat profile across the heated region and the refractive index map are shown in Figure 3a-b, respectively (the simulation parameters, geometry and boundary conditions are described in the supplementary file). The threshold damage temperature of 86^0 C is reached after absorption of more than 0.3 mJ (see Figure 3a), at which we still measured a nearly optimal focus (see Figure 2d).

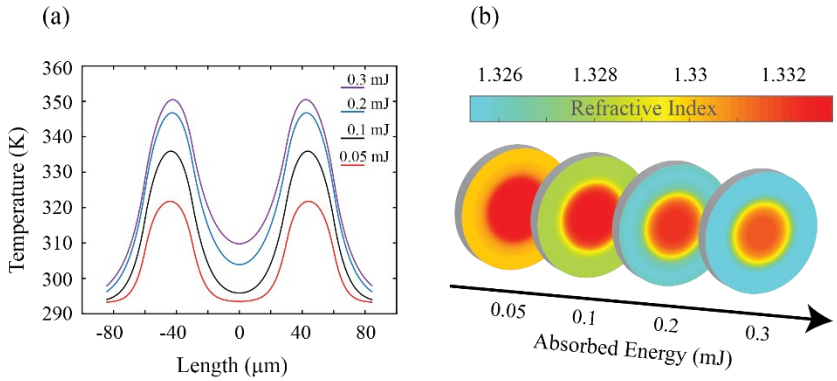

Fig. 3: (a) Simulated heat profile of a cross-section of the ring for different energy absorption values. (b) Corresponding refractive index maps.

CONCLUSIONS

As a result, we have demonstrated a method to sculpt transient microlenses within samples and obtain sub-diffraction focusing without any additional optical element or exogenous label. Our method is compatible with nearly any imaging or focusing optical configuration and thus we expect that it can be broadly adopted in many applications by using ultrafast lasers.

METHODS

Sample preparation: To enhance the absorption at our available wavelength of 1064 nm we fabricated a custom absorbing chamber and placed it before the object. As an absorbing material we used a dilution of 1 % of an absorbing dye (QCR Solution Corp, NIR1054B) in water. This process is needed when absorption is not sufficient due to lack of laser intensity or a mismatch between the material absorption and the operating wavelength.

Imaging process: The object was placed behind the absorbing chamber at a plane where the vertically induced focal point is obtained. A two-dimensional motorized scanning stage was used for lateral scanning, and a sCMOS camera (Andor Zyla 4.2) was placed behind the object to collect the transmitted light. The stage was synchronized with the camera and an optical chopper to ensure that the camera will capture the intensity generated by a single transient optical pulse at every location of the object. The intensity of the final image for each pixel was determined by the integration over a selected surface of the camera.

Simulation parameters: The simulation was performed using the heat diffusion model of COMSOL; a ring shaped profile with a $30\ \mu m$ radius and $30\ \mu m$ thickness was assumed to absorb 0.075 W of power, the dimensions were set to match our experimental conditions. Boundary conditions were set to room temperature far away from the heated region, and the varying heat profile was modeled at time intervals of 0.1 ms.

ASSOCIATED CONTENT

Supporting Information

Mathematical derivation of the heat induced focusing; Absorption spectra of the NIR absorbing dye; Details and results of the COMSOL heat diffusion simulation.

ACKNOWLEDGMENTS

This work was funded in part by the Maryland Catalyst Fund and by National Science Foundation Grants CMMI 1929412 and CBET 1935817.

REFERENCES

(1) Betzig, E.; Patterson, G. H.; Sougrat, R.; Lindwasser, O. W.; Olenych, S.; Bonifacino, J. S.; Davidson, M. W.; Lippincott-Schwartz, J.; Hess, H. F. Imaging intracellular fluorescent proteins at nanometer resolution. *Science* **2006,** *313* (5793), 1642-1645.

(2) Hess, S. T.; Girirajan, T. P.; Mason, M. D. Ultra-high resolution imaging by fluorescence photoactivation localization microscopy. *Biophysical journal* **2006,** *91* (11), 4258-4272.

(3) Hell, S. W.; Wichmann, J. Breaking the diffraction resolution limit by stimulated emission: stimulated-emission-depletion fluorescence microscopy. *Optics letters* **1994,** *19* (11), 780-782.

(4) Huang, B.; Babcock, H.; Zhuang, X. Breaking the diffraction barrier: super-resolution imaging of cells. *Cell* **2010,** *143* (7), 1047-1058.

(5) Li, Y.; Liu, X.; Li, B. Single-cell biomagnifier for optical nanoscopes and nanotweezers. *Light: Science & Applications* **2019,** *8* (1), 61.

(6) Jang, M.; Horie, Y.; Shibukawa, A.; Brake, J.; Liu, Y.; Kamali, S. M.; Arbabi, A.; Ruan, H.; Faraon, A.; Yang, C. Wavefront shaping with disorder-engineered metasurfaces. *Nature Photonics* **2018**, 1.

(7) Vellekoop, I. M.; Lagendijk, A.; Mosk, A. P. Exploiting disorder for perfect focusing. *Nature Photonics* **2010,** *4* (5), 320-322, DOI: 10.1038/nphoton.2010.3.

(8) Veselago, V. Electrodynamics of substances with simultaneously negative and. *Usp. Fiz. Nauk 92*, 517.

(9) Pendry, J. B. Negative refraction makes a perfect lens. *Physical review letters* **2000,** *85* (18), 3966.

(10) Fang, N.; Lee, H.; Sun, C.; Zhang, X. Sub–diffraction-limited optical imaging with a silver superlens. *Science* **2005,** *308* (5721), 534-537.

(11) Wang, Z. B.; Guo, W.; Li, L.; Luk'yanchuk, B.; Khan, A.; Liu, Z.; Chen, Z. C.; Hong, M. H. Optical virtual imaging at 50 nm lateral resolution with a white-light nanoscope. *Nature Communications* **2011,** *2*, DOI: 10.1038/ncomms1211.
(12) Darafsheh, A.; Walsh, G. F.; Dal Negro, L.; Astratov, V. N. Optical super-resolution by high-index liquid-immersed microspheres. *Applied Physics Letters* **2012,** *101* (14), DOI: 10.1063/1.4757600.
(13) Zhang, X.; Liu, Z. Superlenses to overcome the diffraction limit. *Nature materials* **2008,** *7* (6), 435.
(14) Boyd, R. W. Nonlinear Optics, 3rd Edition. *Nonlinear Optics, 3rd Edition* **2008**, 1-613.
(15) Born, M.; Wolf, E. *Principles of optics: electromagnetic theory of propagation, interference and diffraction of light*, Elsevier: 2013.
(16) Gordon, J.; Leite, R.; Moore, R. S.; Porto, S.; Whinnery, J. Long-transient effects in lasers with inserted liquid samples. *Journal of Applied Physics* **1965,** *36* (1), 3-8.
(17) Jhajj, N.; Rosenthal, E.; Birnbaum, R.; Wahlstrand, J.; Milchberg, H. Demonstration of long-lived high-power optical waveguides in air. *Physical Review X* **2014,** *4* (1), 011027.
(18) Chamanzar, M.; Scopelliti, M. G.; Bloch, J.; Do, N.; Huh, M.; Seo, D.; Iafrati, J.; Sohal, V. S.; Alam, M.-R.; Maharbiz, M. M. Ultrasonic sculpting of virtual optical waveguides in tissue. *Nature communications* **2019,** *10* (1), 92.
(19) Scopelliti, M. G.; Chamanzar, M. Ultrasonically sculpted virtual relay lens for in situ microimaging. *Light: Science & Applications* **2019,** *8* (1), 1-15.
(20) Uchiyama, K.; Hibara, A.; Kimura, H.; Sawada, T.; Kitamori, T. Thermal lens microscope. *Japanese Journal of Applied Physics* **2000,** *39* (9R), 5316.
(21) Moreau, J.; Loriette, V. Confocal thermal-lens microscope. *Optics letters* **2004,** *29* (13), 1488-1490.
(22) Long, M.; Swofford, R. L.; Albrecht, A. Thermal lens technique: a new method of absorption spectroscopy. *Science* **1976,** *191* (4223), 183-185.
(23) Helseth, L. Breaking the diffraction limit in nonlinear materials. *Optics communications* **2005,** *256* (4-6), 435-438.
(24) Graciani, G.; Amblard, F. Super-resolution provided by the arbitrarily strong superlinearity of the blackbody radiation. *Nature Communications* **2019,** *10* (1), 1-7.
(25) Yarmolenko, P. S.; Moon, E. J.; Landon, C.; Manzoor, A.; Hochman, D. W.; Viglianti, B. L.; Dewhirst, M. W. Thresholds for thermal damage to normal tissues: An update. *International Journal of Hyperthermia* **2011,** *27* (4), 320-343, DOI: 10.3109/02656736.2010.534527.

For Table of Contents Use Only

Optical focusing beyond the diffraction limit via vortex-assisted transient microlenses

*Eitan Edrei And Giuliano Scarcelli**

Abstract:

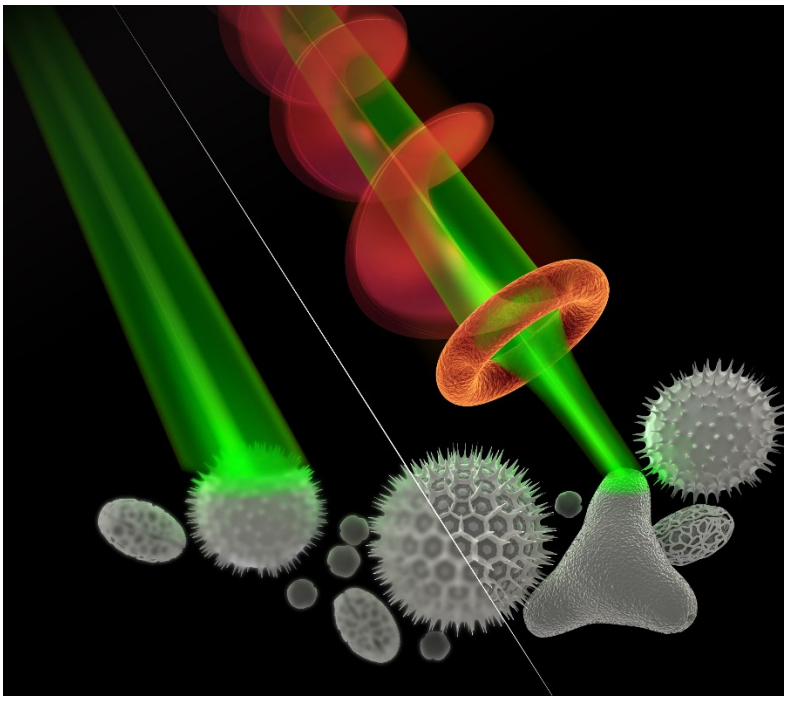

Figure 1:

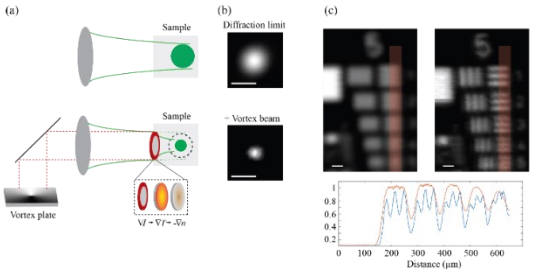

Figure. 1: (a) Schematics of the vortex-assisted focusing. (b) Experimental comparison between the diffraction-limited spot and the one obtained via vortex assisted focusing (Scale Bar, =30 μm). (c) Scanning microscopy image of USAF resolution chart with (left) and without (right) the vortex plate (scale bar = 30

μm). Image resolution is enhanced as can be quantitatively seen from the line plot of the marked region (bottom).

Figure 2:

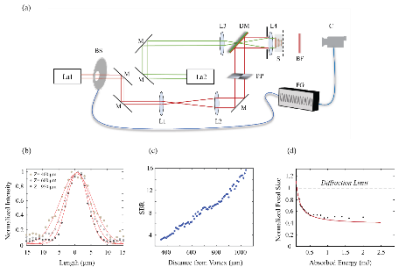

Figure. 2: (a) Experimental setup: Laser (La), Lens (L), Beam Shutter (BS), Function generator (FG), Phase Plate (PP), Dichroic mirror (DM), Sample (S), Filter (BF), Camera (C). (b) Experimental focal spot size at different axial distances from the vortex heat profile (absorbed energy = 1 mJ). (c) SBR values at different axial distances from the vortex heat profile. (d) Focal spot size normalized to the system diffraction limit at increasing energy absorption values (black dots) and a theoretical fit (red line).

Figure 3:

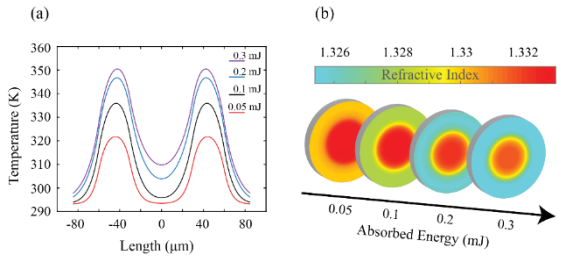

Figure. 3: (a) Simulated heat profile of a cross-section of the ring for different energy absorption values. (b) Corresponding refractive index maps.